

Multicore fiber sensor for high-temperature applications up to 1000°C

J. Enrique Antonio-Lopez,* Zeinab Sanjabi Eznaveh, Patrick LiKamWa, Axel Schülzgen, and Rodrigo Amezcu-Correa

CREOL, The College of Optics and Photonics, the University of Central Florida, Orlando, Florida 32816, USA

*Corresponding author: jealopez@creol.ucf.edu

Received May 2, 2014; revised June 16, 2014; accepted June 20, 2014;
posted June 20, 2014 (Doc. ID 211373); published July 18, 2014

A novel high temperature sensor based on customized multicore fiber (MCF) is proposed and experimentally demonstrated. The sensor consists of a short, few-centimeter-long segment of MCF spliced between two standard single-mode fibers. Due to interference effects, the transmission spectrum through this fiber chain features sharp and deep notches. Exposing the MCF segment to increasing temperatures of up to 1000°C results in a shift of the transmission notches toward longer wavelengths with a slope of approximately 29 pm/°C at lower temperatures and 52 pm/°C at higher temperatures, enabling temperature measurements with high sensitivity and accuracy. Due to its compact size and mechanical rigidity, the MCF sensor can be subjected to harsh environments. The fabrication of the MCF sensor is straightforward and reproducible, making it an inexpensive fiber device. © 2014 Optical Society of America

OCIS codes: (060.2280) Fiber design and fabrication; (060.2370) Fiber optics sensors; (280.4788) Optical sensing and sensors; (280.6780) Temperature.

<http://dx.doi.org/10.1364/OL.39.004309>

Over the years, optical fiber sensors have attracted growing interest for many industrial applications because they offer attractive features such as miniaturization, immunity to electromagnetic radiation, high stability and reliability, extraordinary resistance to corrosive environments, and the possibility of remote interrogation from long distances [1]. All of these characteristics are highly desirable for applications in harsh environments where accurate measurements of physical parameters are required for safe and efficient operation and control. Examples where temperatures need to be measured under extreme conditions include down-hole drillings for oil and gas exploration, power plant turbines, and aircraft engines. Therefore, a large variety of fiber optic temperature sensors based on single-mode fiber (SMF) configurations and special fibers have been envisioned and demonstrated [2–13] to be able to operate at high temperatures. These sensors use multimode fibers, photonic crystal fibers (PCF), microcavities and microchannel, microstructured and twin-core fibers, to mention a few. For high-temperature measurements, special emphasis has been put on sensors based on PCFs [5–9]. However, such PCF configurations present several challenges and disadvantages. For instance, they usually have high insertion loss and very low fringe visibility. In addition, sometimes PCF-based sensing schemes require complex fabrication processes to produce special structures increasing the complexity and final cost of the sensor device. Similarly, microcavities fabricated on capillary fiber tips, microchannel-drilled fiber cores [10,11], as well as microstructured fiber tapers [5,12] require complicated fabrication processes such as laser micromachining or chemical etching which make them difficult to reproduce, hard to integrate and expensive. Furthermore, they suffer from low sensitivity, and in some cases, exhibit a limited measurement range. Another important alternative for high-temperature measurements are regenerated fiber Bragg gratings. Despite being an attractive alternative, they exhibit some gradual deterioration of its spectral features

and involve complicated and possibly expensive fabrication processes [13].

Recently, twin-core fiber devices have been explored as an attractive candidate to accurately measure elevated temperatures [14]. The proposed sensor utilizes a twin-core fiber length of 4 cm directly spliced between two SMFs. The maximum temperature measured with this sensor is 700°C which is not sufficient for many of the aforementioned applications. Here, we present a novel and very stable multicore fiber (MCF)-based sensor that is capable of accurate measurements of temperatures of up to 1000°C. Compared to the twin-core device, the proposed MCF sensor shows significant improvements in terms of signal strength, accuracy, and polarization insensitivity. Furthermore, this MCF presents a symmetric core distribution, making it a polarization-independent fiber device. The fabrication of this MCF sensor is simple and relatively cost effective, resulting in a very promising device for many other applications.

A schematic of the sensor is shown in Fig. 1. The sensor is fabricated by splicing a short, few-centimeter-long segment of MCF between two standard SMFs [see Fig. 1(d)]. The measurement principle is mode interference within the MCF segment, which results in deep notches in the transmission spectra shown in Fig. 2. With

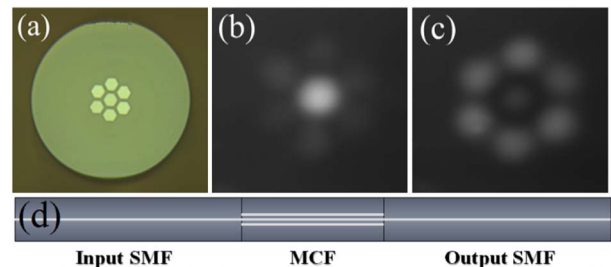


Fig. 1. (a) Cross-section image of the MCF. (b) and (c) Light distributions at different positions along the seven-core fiber axis. (d) Schematic diagram of the interferometric fiber sensor.

increasing temperatures, the spectral positions of these notches shift to longer wavelengths due to changes in refractive indices and thermal expansion. The sensitivity of the interferometric measurement scheme provides accuracy and high resolution, while the compact device structure results in stability, reproducibility, and reliability up to the highest temperatures that the base glass can be exposed to. The key element in our sensor device is the MCF segment. In this study, the MCF applied to fabricate the sensor contains seven strongly coupled Ge-doped cores embedded in a pure silica background. A cross-section image of this MCF is shown in Fig. 1(a). The seven cores have diameters of about $9\ \mu\text{m}$ and numerical apertures of 0.142, and the cladding diameter is $120\ \mu\text{m}$.

The MCF device is fabricated by splicing a small section of this 7-core fiber between two segments of SMF-28, which act as the input and output ports for the light. When light is launched from the SMF into the MCF, several modes can be excited. Due to the MCF symmetry, only two supermodes of the MCF are excited by the fundamental mode of the input SMF at center-core excitation. As light propagates down the length of the MCF segment, the interference between the two excited modes results in continuously varying spatial patterns along the fiber axis. Two of those patterns calculated for two different positions are shown in Figs. 1(b) and 1(c) illustrating the cross-coupling between central and surrounding cores during propagation.

In the spectral domain, the multimode interference in the MCF segment produces a periodic modulation of the transmission measured through the SMF–MCF–SMF device. The spectral periodicity of the transmission signal strongly depends on the length of the MCF segment. As is shown in Fig. 2, a 1 cm MCF segment produces only one deep notch around 1537 nm within the range between 1450 and 1650 nm. In contrast, several deep notches at various wavelengths can be observed for MCF segments of 2 and 3 cm length. Between notches, high transmission is observed indicating almost perfect reconstruction of

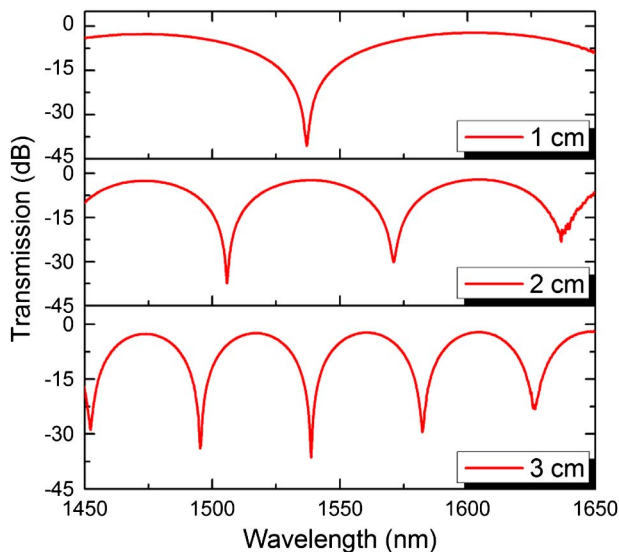


Fig. 2. Measured interference pattern for the proposed device for different MCF lengths.

the launched intensity pattern at the end of the MCF segment for these wavelengths.

Physical external changes affect the MCF interference pattern causing the transmission spectrum to shift in wavelength. Tracking these wavelength shifts allows for accurate and reliable measurements of external perturbations in real time. Since the refractive index depends on the temperature through the thermo-optic effect and thermal expansion or contraction takes place, the interference pattern depends also on the temperature. In order to demonstrate the MCF-based temperature sensor functionality, a device with a 2 cm MCF segment was tested. The sensor was placed in a horizontal tube furnace by Lindberg, and its transmission was monitored. To do so, light from a superluminescent diode (SLD 1550S-A1) with a wavelength range from 1550 to 1650 nm was coupled into the SMF input port. After propagation through the sensor, the transmitted light exiting from the SMF output port was monitored by an optical spectrum analyzer (OSA) by Agilent.

In order to avoid any impact induced by bending, the input and output SMF ends were fixed outside of the furnace to keep the sensor straight. With the purpose of eliminating all the residual stress in the MCF that has been accumulated during the fiber drawing phase [15], the device was first subjected to a long annealing process, being heated up to 1000°C and maintained at this temperature for about 10 h. It was then passively cooled down until it reached room temperature [7,15]. At room temperature, this device features a deep transmission notch close to 1569 nm. During the annealing process, an expected red shift was observed up to 1000°C . At 1000°C , a red shift was observed during the first few minutes of annealing followed by a blue shift despite the constant temperature of 1000°C . After about 6 h of annealing at 1000°C , the sensor transmission spectrum stabilized and remained stable throughout the final 4 h.

After the annealing process, the sensor was tested stepwise by heating up and cooling down the furnace. Figure 3 shows the spectral response of the MCF sensor for 100°C increments changed in 30-minute intervals. As expected, the wavelength of the deep notch shifts to longer wavelengths as the temperature is increased. Between room temperature and 1000°C , the transmission

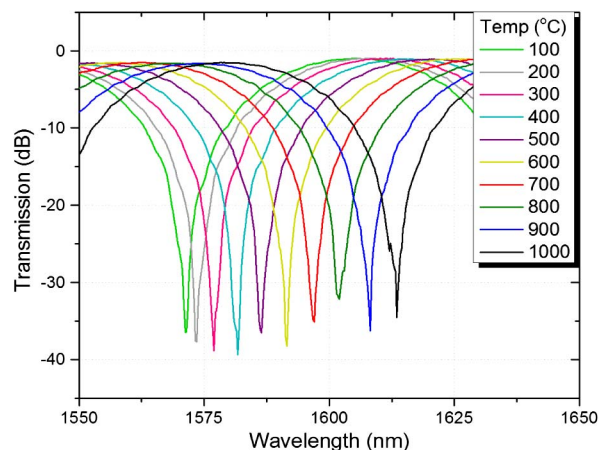


Fig. 3. Superimposed spectral response of a sensor with 2 cm of 7-core fiber as a function of temperature.

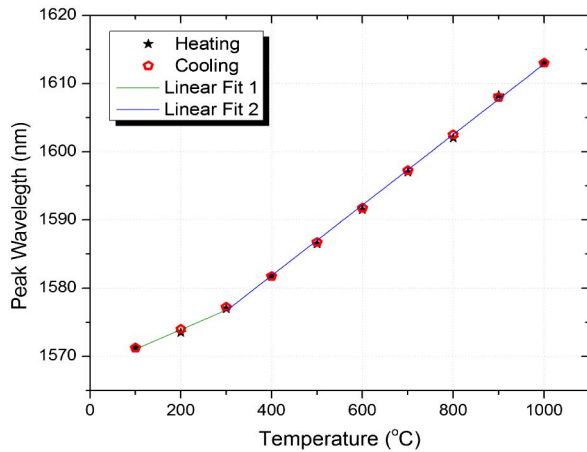


Fig. 4. Maximum attenuation peak of the wavelength versus temperature variation for the heating and cooling cycle.

minimum shifts a total of 43.5 nm, from 1469 to 1613.5 nm. The insertion loss of the MCF device and the fringe visibility were obtained as 1 and 37 dB, respectively, which outperforms most of the sensors based on interference effects reported so far.

Figure 4 shows the wavelength shift of the transmission minimum versus temperature. The black stars and the red pentagons have been measured during the heating and the cooling cycle, respectively. Data points for increasing and decreasing temperatures match very well for all temperatures, showing no thermal hysteresis of the MCF device. This stable and accurate performance up to the highest temperatures should be attributed to the successful annealing process, which eliminates residual stress and thermal memory. As shown in Fig 4, the sensor response can be approximated by two linear fits of the transmission minimum shift with temperature, for two temperature ranges. For the temperature range of 100°C–300°C, a shift of ~ 28.7 pm/°C is obtained. For higher temperatures in the range of 300°C–1000°C, a sensitivity of ~ 51.7 pm/°C is obtained. More accurate calibration can be performed to account for the variations of thermo-optic effects with temperature.

In order to demonstrate the reproducibility and accuracy of the response of the MCF temperature sensor, the heating and cooling cycle was repeated three times with the same steps and under the same conditions. During all of these cycles, a maximum variation of less than 2% in a temperature-induced shift has been measured and no hysteresis has been observed during any of the tests. This further emphasized the repeatability and reliability of the MCF sensor performance during high-temperature measurements.

To further prove the sensor's stability at high temperatures, the sensor was exposed to 1000°C for 5 h and subsequently passively cooled down in 100°C steps. Figure 5 shows the time evolution of the wavelength (red spheres) and temperature shift (blue line) as the MCF was heated, kept at 1000°C, and cooled down to room temperature. A very stable response from the sensor was observed at long time measurements under high-temperature conditions. It is very important to highlight that this heating was kept at 1000°C and the cooling cycle was also repeated three times, obtaining the same results each time

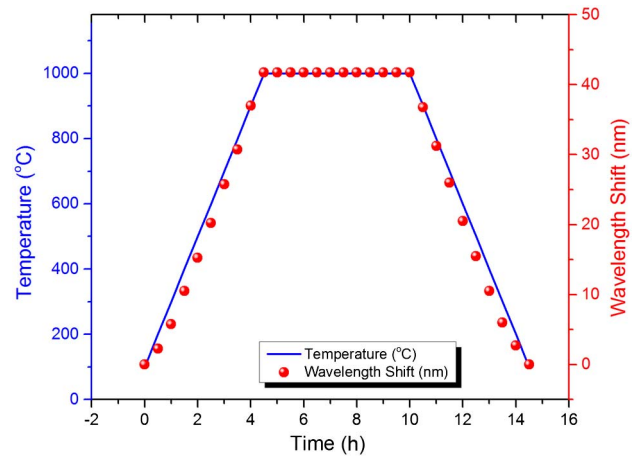


Fig. 5. Time evolution of the wavelength shift of the MCF sensor (red dots) during a long cycle of temperature variations (blue line).

for all tests. Figure 5 also shows that during the complete cycle, the MCF sensor exhibited a maximum wavelength deviation of ~ 0.5 nm, equivalent to 9.6°C.

In conclusion, we have demonstrated a very simple sensor device with highly stable performance based on a Ge-doped seven-core fiber that provides sharp spectral features due to mode interference effects suitable for optical interrogation. The high stability and repeatability of the sensor were corroborated keeping for 5 h at 1000°C and performing several thermal cycling experiments. We have demonstrated the reproducibility of temperature measurements with an error of less than 2%. Between 100°C and 1000°C, the sensitivity of our device is ~ 52 pm/°C. This type of sensor is very promising due to its high sensitivity and simple fabrication process, resulting in a fiber device with reproducibility, reliability, compactness, and low cost. Our new approach to MCF-based high-temperature sensors compares favorably with other high-temperature fiber sensors, however, at reduced levels of complexity in fabrication and operation.

J. Enrique Antonio-Lopez would like to thank the Mexican Council of Science and Technology (CONACyT) for the postdoctoral scholarship granted to him.

References

1. F. T. S. Yu, P. B. Ruffin, and S. Yin, *Fiber Optic Sensors* (CRC Press, 2008).
2. E. Milcent, G. Olalde, J. F. Robert, D. Hernandez, and M. Clement, *Appl. Opt.* **33**, 5882 (1994).
3. S. H. Nam and S. Yin, *IEEE Photon. Technol. Lett.* **17**, 11 (2005).
4. E. Li, X. Wang, and C. Zhang, *Appl. Phys. Lett.* **89**, 9 (2006).
5. D. Monzon-Hernandez, V. P. Minkovich, and J. Villatoro, *IEEE Photon. Technol. Lett.* **18**, 511 (2006).
6. H. Y. Choi, K. S. Park, S. J. Park, U. C. Paek, B. H. Lee, and E. S. Choi, *Opt. Lett.* **33**, 21 (2008).
7. G. Coviello, V. Finazzi, J. Villatoro, and V. Pruneri, *Opt. Express* **17**, 21551 (2009).
8. S. M. Nalawade and H. V. Thakur, *IEEE Photon. Technol. Lett.* **23**, 1600 (2011).
9. B. Park, J. Provine, W. Jung, R. T. Howe, and O. S. Solgaard, *IEEE Sens. J.* **11**, 11 (2011).

10. J. Ma, J. Ju, L. Jin, W. Jin, and D. Wang, *Opt. Express* **19**, 13 (2011).
11. Y. Liu, S. Qu, and Y. Li, *Opt. Lett.* **38**, 3 (2013).
12. G. Statkiewicz-Barabach, J. P. Carvalho, O. Frazao, J. Olszewski, P. Mergo, J. L. Santos, and W. Urbanczyk, *Appl. Opt.* **50**, 3742 (2011).
13. S. Li-Yang, T. Wang, J. Canning, K. Cook, and T. Hwa-Yaw, *Appl. Opt.* **51**, B30 (2012).
14. P. Rugeland and W. Margulis, *Appl. Opt.* **51**, 6227 (2012).
15. Y. Mohanna, J. M. Saugrain, J. C. Rousseau, and P. Ledox, *J. Lightwave Technol.* **8**, 1799 (1990).